JACS
JOURNAL OF THE AMERICAN CHEMICAL SOCIETY
Article
pubs.acs.org/JACS

Unraveling the ^{13}C NMR Chemical Shifts in Single-Walled Carbon Nanotubes: Dependence on Diameter and Electronic Structure

Chaiwat Engtrakul,*[,#] Veronica M. Irurzun,[‡] Erica L. Gjersing,[#] Josh M. Holt,[#] Brian A. Larsen,[#] Daniel E. Resasco,[‡] and Jeffrey L. Blackburn*[,#]

[#]National Renewable Energy Laboratory, 1617 Cole Boulevard, Golden, Colorado 80401, United States

[‡]School of Chemical, Biological, and Materials Engineering, University of Oklahoma, Sarkeys Energy Center, Norman, Oklahoma 73019, United States

Supporting Information

ABSTRACT: The atomic specificity afforded by nuclear magnetic resonance (NMR) spectroscopy could enable detailed mechanistic information about single-walled carbon nanotube (SWCNT) functionalization as well as the noncovalent molecular interactions that dictate ground-state charge transfer and separation by electronic structure and diameter. However, to date, the polydispersity present in as-synthesized SWCNT populations has obscured the dependence of the SWCNT ^{13}C chemical shift on intrinsic parameters such as diameter and electronic structure, meaning that no information is gleaned for specific SWCNTs with unique chiral indices. In this article, we utilize a combination of ^{13}C labeling and density gradient ultracentrifugation (DGU) to produce an array of ^{13}C-labeled SWCNT populations with varying diameter, electronic structure, and chiral angle. We find that the SWCNT isotropic ^{13}C chemical shift decreases systematically with increasing diameter for semiconducting SWCNTs, in agreement with recent theoretical predictions that have heretofore gone unaddressed. Furthermore, we find that the ^{13}C chemical shifts for small diameter metallic and semiconducting SWCNTs differ significantly, and that the full-width of the isotropic peak for metallic SWCNTs is much larger than that of semiconducting nanotubes, irrespective of diameter.

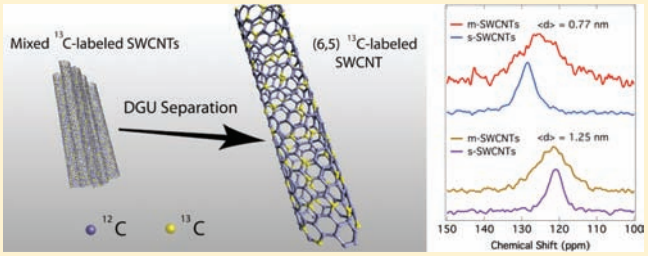

1. INTRODUCTION

For the π aromatic allotropes of carbon, e.g., fullerenes, single-walled carbon nanotubes (SWCNTs), and graphene/graphite, the ^{13}C nuclear magnetic resonance (NMR) spectrum is a unique chemical signature that can relay critical information on bond hybridization, density of states, curvature, and coupling to nuclear spins of adjacent molecules. ^{13}C NMR has been a critical tool for identifying unique fullerenes (e.g., C_x, where x = 56, 60, 70, 78), confirming the symmetry of particular fullerene isomers,[1] tracking functionalization reactions of the fullerene sidewall,[2,3] and analyzing endohedral fullerenes.[4] ^{13}C NMR has also been used to characterize both covalent SWCNT sidewall functionalization[5−7] and noncovalent interactions such as the interaction with encapsulated water.[8] However, the same level of chemical specificity achieved for fullerenes has not been attained for SWCNTs because of the polydispersity present in as-produced SWCNT samples.

Recent advances in the separations of SWCNTs by electronic structure, diameter, and even chirality (left- versus right-handed) have been achieved by the clever utilization of surfactants to affect SWCNT properties such as density[9,10] or mobility through a fractionating column.[11−13] Such separations have initiated a new era of SWCNT research, in which highly enriched samples can shed light on the molecular-level properties of unique SWCNTs. SWCNT electronic structure varies as a function of diameter (d) and chiral angle, properties captured in the unique chiral indices (n,m) of each SWCNT. Nanotube properties follow patterns based on the nanotube family (λ), determined by the relationship

$$2n + m = 3p + \lambda \quad (1)$$

where n and m are the chiral indices of a particular SWCNT and p is an integer. Two thirds of SWCNTs are in the λ = 1 and λ = 2 families and are semiconducting (s-SWCNTs), while the other one third, in the λ = 0 family, are metallic or semimetallic (m-SWCNTs).[14] For over a decade, theoretical calculations have predicted that the ^{13}C chemical shift of a SWCNT should depend sensitively on diameter and electronic structure,[15−20] but the polydispersity of as-produced SWCNT samples has precluded validating these computations. Whereas fullerene ^{13}C NMR can be said to yield truly molecular-level information, SWCNT ^{13}C NMR has remained at the materials level, with no unequivocal information on the relation of the observed ^{13}C NMR spectrum to SWCNTs with specific chiral indices, diameters, or electronic structures. Only one recent report has examined the dependence of the ^{13}C chemical shift on SWCNT electronic structure, within a narrow diameter range.[21] Another

Received: November 29, 2011
Published: February 14, 2012

   dx.doi.org/10.1021/ja211181q | J. Am. Chem. Soc. 2012, 134, 4850−4856

recent report examined the effect of diameter and wall number on the ^{13}C chemical shift.[22]

Beyond the fundamental importance of understanding the intrinsic magnetic properties of SWCNTs, ^{13}C-labeled SWCNTs with well-characterized electronic structure could enable detailed investigations into important covalent and noncovalent SWCNT interactions. For example, the simple concept of utilizing ^{13}C-labeled SWCNTs in separation processes outlined in this study should allow for a detailed probe of the interfacial coupling of unique SWCNT species with the molecules used for separation, thus enabling predictive models for the molecular archetypes that will yield highly selective and efficient separations. Such samples may also enable unequivocal identification of sidewall functional groups, such as endoperoxides, that have been theoretically predicted to control SWCNT optical and electrical properties.[23,24] Finally, as a technological example, SWCNTs are being explored as potential absorbers and electron acceptors in organic photovoltaic composites with semiconducting polymers.[25,26] It has been demonstrated experimentally that the excited-state charge carrier dynamics in such composites depend sensitively on the SWCNT electronic structure.[26] However, very little is known experimentally about the atomic structure at the polymer−SWCNT interface and how this interfacial structure varies with SWCNT electronic structure or diameter. Several recent investigations have used two-dimensional (2D) NMR to probe molecular ordering, domain size, and composite morphology in organic photovoltaic (OPV) composites of semiconducting polymers and fullerenes.[27,28] Because excited-state interactions such as electron/hole transfer are ultimately dictated by this ground-state interfacial structure, using 1D- and 2D-NMR to gain a detailed knowledge of how polymers interface with SWCNTs of known electronic structure could aid in the rational design of better SWCNT OPV active layers.

In this article, we combine the advantages of highly enriched samples separated by electronic structure and diameter with ^{13}C labeling to enhance the sensitivity and spectral resolution in solid-state NMR spectroscopy of SWCNTs. The unprecedented range of highly enriched, well-characterized ^{13}C-labeled SWCNT samples produced here allows us to rigorously address the theoretically predicted dependence of ^{13}C chemical shift on SWCNT diameter and electronic structure. We utilize absorbance, Raman, and photoluminescence spectroscopies to thoroughly characterize the diameter and electronic structure variations for ^{13}C-labeled SWCNTs separated by density gradient ultracentrifugation. Subsequent characterization by solid-state magic angle spinning (MAS) NMR demonstrates that the isotropic ^{13}C chemical shift for semiconducting SWCNTs systematically decreases with increasing diameter, with a functional form that is well characterized by recent first principle calculations.[17] The ^{13}C chemical shifts for small diameter metallic and semiconducting SWCNTs are found to differ significantly, while for larger diameter SWCNTs they are nearly equivalent. Finally, the full-width of the isotropic peak for metallic SWCNTs is much larger than that of semiconducting nanotubes, irrespective of diameter, a trend that to our knowledge has not been captured by theoretical calculations.

2. EXPERIMENTAL DETAILS

SWCNT Synthesis. Small diameter SWCNTs were produced by following the CoMoCAT process.[29−31] Briefly, 1 g of calcined catalyst was set into a vertical quartz reactor of 1/2 in. diameter and prereduced under H_2 (300 sccm) for 30 min at 545 °C. Subsequently, the temperature was raised to 680 °C under He (300 sccm). Carbon monoxide (300 sccm) was finally fed at 680 °C for 30 min. ^{13}C-Labeled SWCNTs were produced by using a mixed gas feed of ultrahigh purity ^{12}CO and ^{13}CO (Cambridge Isotope Laboratories, Inc.) with a ^{13}C partial pressure of 0.2. Pure ^{12}C and ^{13}C SWCNT were also synthesized for comparison. The as-produced samples were purified by acidic treatments and a series of oxidation steps.

Large diameter SWCNTs were prepared by laser vaporization (LV) of a graphite target containing 3% (by weight) each of nickel and cobalt catalysts.[32] The ^{12}C graphite utilized in the target was 7−10 μm graphite purchased from Aldrich. For ^{13}C syntheses, 20% of the graphite was replaced with amorphous ^{13}C (Cambridge Isotope Laboratories, Inc.), as described previously.[21,33,34] No further purification was performed before dispersion of the LV SWCNTs for density gradient ultracentrifugation (DGU) separation.

Density Gradient Ultracentrifugation. Several different DGU experiments were performed to achieve the range of samples analyzed in this study. Small-diameter CoMoCAT SWCNTs with three different ^{13}C labeling levels (0%, partially labeled, and 100%) were subjected to a single-surfactant separation to achieve separation by both diameter and electronic structure.[9] For this separation, purified CoMoCAT SWCNTs were dispersed in 2% aqueous sodium cholate by sonication at 30% with a 1/4 in. ultrasonic tip (Cole Parmer, 750 W) for 1 h. This dispersion was not centrifuged prior to separation by DGU. The SWCNT dispersion was then blended with a 60% iodixanol solution (Optiprep density gradient medium) to produce a dispersion with ∼24% iodixanol. This dispersion was injected into a linear density gradient that varied from 7.5% and 22.5% iodixanol with 2% sodium cholate. DGU separation was achieved by centrifuging at 41 000 rpm (207 570g average centripetal force, 288 244g maximum centripetal force) in an SW-41 rotor for 12 h at 20 °C. This DGU separation leads to a thick, dark purple band that lies near the middle of the centrifuge tube above a much larger dark gray band that extends almost to the bottom of the centrifuge tube. The bottom layer of the separation, ∼1/2 in. above the bottom of the tube, consists of a dense mat of either bundled SWCNTs and/or SWCNTs to which residual catalyst metals are attached. Four fractions (F1−F4) were removed from the centrifuge tube, with the bottom fraction (F4) being removed from approximately 1 in. above the lowest-lying dense mat. This was done to ensure that all fractions did not contain appreciable amounts of residual catalyst metals that would broaden NMR peaks.

Both ^{13}C-labeled LV SWCNTs and CoMoCAT were subjected to a cosurfactant DGU separation that enables enrichment primarily by electronic structure.[9,21] Small diameter CoMoCAT SWCNTs were only subjected to a DGU separation tailored for extraction of enriched m-SWCNTs as the most buoyant fraction. For this separation, the SWCNTs are first sonicated in a 1% sodium cholate (SC) solution (30% power, 1 h). Then, sodium dodecyl sulfate (SDS) was added to bring the total concentration of surfactant up to 2% while achieving a 3:2 ratio of SDS:SC by weight. The density gradient for m-SWCNT separation ranged from 20% to 35% iodixanol, and m-SWCNT separation was achieved by 16 h of centrifugation at 41 000 rpm and 12 °C. After centrifugation, the CoMoCAT m-SWCNTs were extracted as a thick yellow band near the middle of the centrifuge tube. LV SWCNTs were subjected to the same conditions for m-SWCNT separation. The LV m-SWCNTs were extracted as a thick blue band near the middle of the centrifuge tube. LV SWCNTs were also subjected to a DGU separation tailored for s-SWCNT enrichment as the most buoyant fraction. The cosurfactant mixture for s-SWCNT enrichment was 4:1 SC:SDS (2% total surfactant concentration). DGU enrichment was performed in an SW-41 rotor (LX-100P Beckman centrifuge) at a speed of 41 000 rpm. S-SWCNT enrichment was achieved by 16 h of centrifugation at 41 000 rpm and 25 °C.

Preparation of Solid-State NMR Samples. Solid-state samples were prepared for ^{13}C NMR by filtering a particular enriched SWNT dispersion through a 0.05 μm mixed cellulose ester (MCE) filter. Following filtration, the enriched SWNT buckeypaper was rinsed with ∼50 mL of DI water to remove excess surfactant and iodixanol. The filter and buckeypaper were then removed and placed into a beaker of

acetone to dissolve the MCE filter. After ~16 h, the buckeypaper was removed and placed in another beaker of acetone to ensure full dissolution and removal of the MCE. The enriched buckeypaper was then subjected to mild heating in vacuum to remove surface-bound molecules. This degas step was performed by folding the buckeypaper into a preweighed platinum packet that was then placed into a quartz tube (fitted with a valve) that is custom-made for temperature-programmed desorption (TPD) experiments. This sample holder was then attached to the TPD apparatus and evacuated to a base pressure of ~3 × 10^{-8} Torr. A tube furnace placed around the quartz tube heated the sample to 200 °C over 1 h while molecular desorption was monitored with a mass spectrometer. Following this degas step, the platinum packet and sample were reweighed to determine the mass of the buckeypaper to be measured in the NMR experiment. The Mettler Toledo microbalance used to measure the platinum and samples masses has an accuracy of 0.1 μg. The masses of samples measured in these experiments ranged from ~100 to 600 μg.

^{1}H−^{13}C CP-MAS experiments were performed on various SWCNT samples that were soaked in 4 M NaOH for seven days at room temperature. After being soaked in base, SWCNT samples were dried briefly under ambient conditions.

MAS Solid-State NMR. High-resolution, solid-state ^{13}C NMR spectra were collected on a Bruker Avance 200 MHz spectrometer (4.7 T) operating at 50.13 MHz for ^{13}C at room temperature, with MAS rotation rates of 7 kHz under a nitrogen atmosphere. The spectra were acquired under high-power proton decoupling using a $\pi/2$ pulse length of 5.2 μs and a recycle delay of 10 s and were referenced to adamantane (spectra acquired over ~98 h). NMR samples were loaded into zirconium oxide rotors (7 mm outer diameter) and packed between two plugs of either polyethylene or Teflon under ambient conditions. Polyethylene plugs were used in single pulse experiments and Teflon plugs in ^{1}H−^{13}C CP-MAS experiments in order to minimize background signals, balance the rotor, center the small amount of SWCNT sample in the NMR coil, and provide a barrier against exposure to ambient conditions. The feature at 139 ppm in the ^{13}C NMR spectra (e.g., Figure 3a) is due to unsaturated impurities in the polyethylene plugs. CP experiments on the F1-CoMoCAT sample were carried out at room temperature using a 5 ms contact time, spinning rate of 7 kHz, and a pulse repetition rate of 1.0 s (spectra acquired over ~43 h). CP experiments on the MF1-CoMoCAT SWCNTs and LV SWCNTs (94% metallic and 92% semiconducting) were carried out on a Bruker Avance III 600 MHz spectrometer (14.09 T) operating at 150.9 MHz for ^{13}C at room temperature (zirconium oxide rotors, 3.2 mm outer diameter). The spectra were obtained under high-power proton decoupling using a $\pi/2$ pulse length of 3.4 μs, 5 ms contact time, spinning rate of 15 kHz, and pulse repetition rate of 1.0 s (spectra acquired over ~43 h). A total of ~300K scans were collected and averaged (spectra acquired over ~86 h) for the MF1-CoMoCAT SWCNT sample because of the low sample mass of ~100 μg.

Raman and Absorption Spectroscopies. Raman spectroscopy was performed on the raw samples (before separation) and the enriched samples after separation. Raman spectra were obtained on unlabeled (99% ^{12}C), 100% ^{13}C-labeled, and partially ^{13}C-labeled liquid-phase dispersions using 20 mW of 2.33 eV (532 nm) laser excitation. Solid-state Raman spectra were obtained using 7 mW of 2.54 eV (488 nm) laser excitation. The slit width was 0.1 mm, allowing for a resolution of 2−4 cm^{-1} across the measured spectrum. Absorbance spectra were performed on a Cary 500 UV−vis-IR spectrometer. Samples were measured in solution phase in 1 cm cuvettes. Photoluminescence excitation (PLE) maps were obtained using a home-built Fourier transform spectrometer described previously.[35]

3. RESULTS AND DISCUSSION

A rigorous analysis of the SWCNT ^{13}C chemical shift first requires a detailed understanding of the polydispersity in both electronic structure and diameter. A detailed analysis of the large diameter SWCNTs synthesized by laser vaporization is presented in our previous communication[21] and is not recounted here for the sake of brevity. For the small diameter SWCNTs synthesized by the CoMoCAT CVD method,[30] we undertook a detailed analysis by absorbance, Raman, and photoluminescence excitation (PLE) spectroscopies. Initially, we performed single-surfactant DGU separations on three CoMoCAT samples containing the naturally occurring ^{12}C:^{13}C ratio (99:1) or labeled with a low level (<20%) or 100% ^{13}C. The top fraction collected from each of these separations was highly enriched with (6,5) SWCNTs, as evidenced by the absorbance spectra in Figure 1a.[36] The absorbance spectrum of

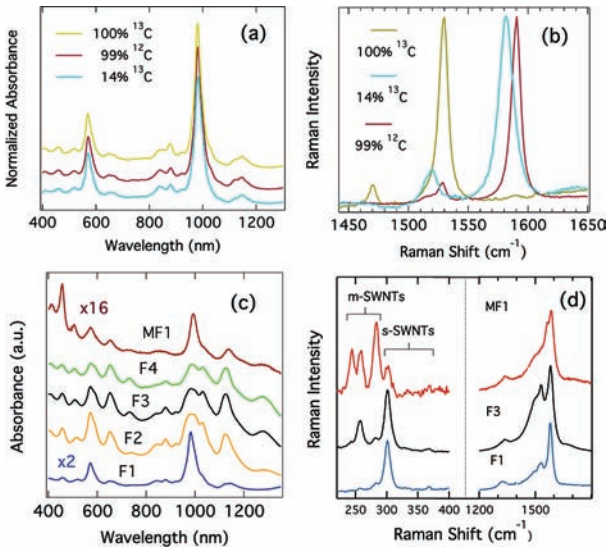

Figure 1. (a) Absorbance spectra of (6,5) enriched CoMoCAT SWCNTs labeled with different levels of ^{13}C, taken after DGU. (b) Solution-phase G band Raman spectra (λ_{exc} = 532 nm) of (6,5) enriched CoMoCAT SWCNTs labeled with different levels of ^{13}C, taken after DGU. (c) Absorbance spectra of the five CoMoCAT ^{13}C-labeled (14% ^{13}C) fractions studied by MAS NMR. (d) Solid-state RBM and G band Raman spectra for samples F1, F3, and MF1 (λ_{exc} = 488 nm).

each sample is dominated by a sharp peak at 980 nm and a smaller peak at 571 nm, representing the first and second excitonic transitions (S_{11} and S_{22}) of (6,5) SWCNTs, respectively.

The isotope-induced softening of the Raman-active E_{1g} mode (G band), shown in Figure 1b, was used to deduce the level of ^{13}C incorporation into the partially ^{13}C-labeled sample that was used for subsequent NMR studies. Replacement of ^{12}C atoms with ^{13}C atoms results in a predictable red shift of the SWNT Raman features because the heavier ^{13}C mass softens the characteristic vibrations. These red shifts are clearly visible in the spectra shown in Figure 1b. The theoretical shift (ω_{13C}) for a sample with a ^{13}C labeling ratio ($m_{13C}/[m_{13C} + m_{12C}]$) of η_{13C} can be calculated by the following relation:

$$\omega_{13C} = \omega_{12C} - [(\omega_{12C} - (\omega_{12C} \times \sqrt{m_{12C}/m_{13C}})) \times \eta_{13C}] \quad (2)$$

where ω_{12C} is the Raman shift for an unlabeled sample and m_{12C} and m_{13C} are the atomic masses of ^{12}C and ^{13}C, respectively. Equation 2 can be rearranged to yield eq 3, which allows for the labeling level to be calculated based on the

dx.doi.org/10.1021/ja211181q | J. Am. Chem. Soc. 2012, 134, 4850−4856

observed Raman shifts for an unlabeled sample and a sample labeled with any level (η_{13C}) of ^{13}C:

$$\eta_{13C} = \frac{\omega_{12C} - \omega_{13C}}{\omega_{12C} - (\omega_{12C} \times 0.9608)} \quad (3)$$

Figure 1b illustrates a Raman shift of 1590.5 cm^{-1} for the G band of the unlabeled (6,5) sample. Equation 3 predicts that the 100% ^{13}C-labeled sample ($\eta_{13C} = 1$) should have a G band shift of 1528 cm^{-1}, in good agreement with the observed shift of 1529.4 cm^{-1}. The partially labeled sample has a G band shift of 1581.5 cm^{-1}, which translates to a ^{13}C level, η_{13C}, of 14% when plugged into eq 3.

Figure 1c compares the absorbance of the five fractions collected from DGU separations of the 14% ^{13}C-labeled CoMoCAT SWCNTs. We note three important regions for the excitonic transitions of these SWCNTs: (1) the S_{11} transitions between ~825 and 1550 nm, (2) the S_{22} transitions between ~515 and 775 nm, and (3) the M_{11} transitions between ~415 and 515 nm. The most buoyant single-surfactant fraction, F1, is highly enriched with small diameter (6,5) SWCNTs, as evidenced by the dominance of one large S_{11} peak at ~980 nm and S_{22} peak at ~571 nm. Each subsequent, less buoyant fraction contained successively broader diameter distributions of s-SWCNTs centered at progressively larger diameters. Because of the overlap of M_{11} and S_{22} peaks for this particular diameter range, it is difficult to precisely discern the contribution of m-SWCNTs to the spectra of fractions F1−F4. However, the cosurfactant separation yields a buoyant yellow band highly enriched with m-SWCNTs, shown in Figure 1c as MF1. The absorbance spectrum of MF1 is dominated by three peaks corresponding to m-SWCNTs in the range of 400−500 nm, in addition to a series of s-SWCNT peaks nearly identical to the peaks found in F1.[36] The similar distribution of s-SWCNT peaks (although with much lower intensity relative to the strong m-SWCNT peaks) suggests that the diameter distribution of MF1 is roughly equivalent to that of F1.

To more precisely examine the distribution of electronic structures (s-SWCNTs versus m-SWCNTs), resonance Raman was performed on the solid-state samples prepared from the dispersions shown in Figure 1c. Figure 1d compares the G band and radial breathing mode (RBM) spectra of samples F1, F3, and MF1. For these samples, the 488 nm excitation wavelength is resonant with the S_{22} transitions of s-SWCNTs with relatively small diameters and for the M_{11} transitions of m-SWCNTs with relatively large diameters. The RBM spectrum of the F1 sample is dominated by one large peak at 304 cm^{-1}, corresponding to the (6,5) SWCNT, along with small shoulders at 290 and 370 cm^{-1} from minority s-SWCNT species.[37] The G band spectrum of the F1 sample displays two sharp peaks at 1592 and 1520 cm^{-1}, corresponding to the G^+ and G^- branches of the G band for s-SWCNTs, respectively.[14] Keeping in mind that the s-SWCNT diameter distribution of MF1 is roughly equivalent to that of F1, significant differences exist in the Raman spectra of MF1 due to the enrichment in m-SWCNTs. A series of peaks in the range of 220 to 290 cm^{-1} correspond to the RBMs of m-SWCNTs,[38] while the 304 cm^{-1} (6,5) RBM peak constitutes only a small shoulder. The G band consists of a sharp peak at 1592 cm^{-1} and a very broad shoulder peaking at ~1520 cm^{-1}, corresponding to the LO and TO branches of the G band of m-SWCNTs, respectively. The RBM peaks for MF1 are analyzed in detail in the Supporting Information to determine precisely which m-SWCNT species are present in this sample.[36] This analysis suggests that the MF1 sample contains the (6,6), (8,5), (7,4), and (11,2) species,[38] although no quantitative information can be determined for the relative concentration of each species. A full comparison of the RBM spectra for F1−F4 in the Supporting Information demonstrates that the weighting of m-SWCNT features systematically increases with increasing fraction number.[36] Collectively, the Raman spectra illustrate that the five ^{13}C-labeled samples produced via DGU span the range of a highly m-SWCNT enriched sample (MF1), to samples of mixed electronic structure (F2−F4), and finally to a sample highly enriched in (6,5) s-SWCNTs (F1).

PLE spectroscopy allows for easier visualization of the individual s-SWCNTs that comprise each sample and affords a rigorous analysis of diameter distributions. Figure 2a and 2b

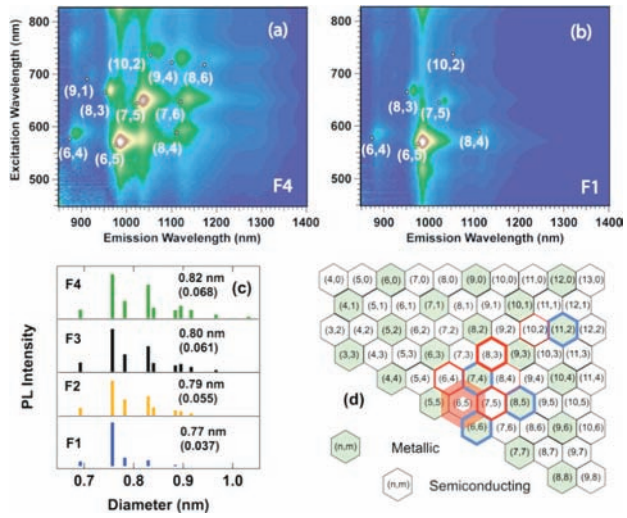

Figure 2. (a) PLE map of sample F4. (b) PLE map of sample F1. (c) PL intensity histogram used to approximate the diameter distribution of samples F1 through F4. The average diameter, $\langle d \rangle$, and standard deviation (Δd, in parentheses) are given for each sample. (d) Section of the graphene lattice with red hexagons highlighting the relative PL intensities of semiconducting SWCNTs present in sample F1. The thickness of the lines are 20, 4.2, 3, 2.5, 1, and 1 for the (6,5), (8,3), (7,5), (6,4), (8,4), and (10,2) SWCNTs, respectively. Blue hexagons highlight the m-SWCNTs identified by resonance Raman spectroscopy for MF1 (see Supporting Information for details). No quantitative information on relative amounts of each species present can be gleaned from Raman or absorbance spectroscopies.

shows photoluminescence excitation (PLE) maps of F4 and F1; the full suite of PLE maps is given in the Supporting Information.[36] The PLE map for F4 shows significant contributions for ten s-SWCNT species, while this distribution is reduced to only six species for F1, with the (6,5) SWCNT dominating the PLE map. Diameter distributions for each fraction were extracted from the PLE maps for correlation with ^{13}C NMR chemical shifts and peak widths. The extracted diameter distributions, shown in Figure 2c, clearly confirm the diameter selection of the DGU separation, with increasing fraction numbers demonstrating progressively broader distributions (Δd) centered at larger average diameters ($\langle d \rangle$). A section of the graphene lattice is given in Figure 2d for easier visualization of the distribution of chiral species in samples F1 and MF1. The thickness of the red hexagons gives the relative weighting for s-SWCNT species in the PL spectrum of F1, while the blue hexagons denote m-SWCNTs identified by the analysis of MF1 RBM peaks.[36] While we cannot definitively determine quantitative weighting for the amounts of m-

dx.doi.org/10.1021/ja211181q | J. Am. Chem. Soc. 2012, 134, 4850−4856

SWCNT species in MF1, it is likely that the sample is dominated by the (6,6) and (7,4) m-SWCNTs because of their proximity to the dominant (6,5) s-SWCNT in the sample.

With the detailed knowledge of electronic structure and diameter for the 14% ^{13}C-labeled SWCNTs in hand, we now turn to the nuclear magnetic resonance spectra. Figure 3a displays the solid-state MAS ^{13}C NMR spectra for the 14% ^{13}C-labeled CoMoCAT samples obtained from DGU separations. The ^{1}H−^{13}C cross-polarization (CP) MAS method has been used previously to obtain significant enhancements in carbon magnetization for SWCNTs under various pH conditions and decrease NMR acquisition time.[33,34] In this study, the CP-MAS method was useful for obtaining high signal-to-noise for samples with relatively small masses (MF1 and LV SWCNTs). Figure 3b shows the ^{1}H−^{13}C CP-MAS spectra for selected CoMoCAT samples and 20% ^{13}C-labeled laser vaporization (LV) synthesized SWCNT samples (94% metallic and 92% semiconducting) after soaking the SWCNT samples in sodium hydroxide and serves to illustrate the effects of electronic structure and diameter. Several interesting trends are immediately obvious from Figure 3. First, as the CoMoCAT fraction number increases from F1 to F4, the ^{13}C chemical shift progressively shifts to lower frequency and the peak envelope broadens (Figure 3a). Second, the spectrum for the metal-enriched MF1 sample is shifted significantly to lower frequency and is very broad relative to fractions F1−F4 (Figure 3b). Finally, the chemical shift of ∼129 ppm for the $\langle d \rangle$ = 0.77 nm (6,5) enriched F1 fraction is shifted to higher frequency relative to the chemical shift typically observed for the most commonly studied large diameter SWCNTs (1.2 < $\langle d \rangle$ < 1.4 nm).[21,33] This difference is clearly illustrated by Figure 3b, which displays the ^{1}H−^{13}C CP-MAS spectra for the DGU-separated LV SWCNTs with $\langle d \rangle$ = 1.25 nm. The LV s-SWCNT (92%) sample exhibits a ^{13}C resonance at ∼121 ppm (fwhm = 5.0 ppm) that is shifted to lower frequency by 8 ppm relative to the smaller diameter (6,5) enriched sample (F1), demonstrating a strong diameter dependence for the ^{13}C chemical shift. The full-width-at-half-maximum (fwhm) for the LV s-SWCNT and F1 samples are ∼5 ppm. To the best of our knowledge, these are the narrowest ^{13}C resonance spectra ever observed for SWCNTs, on the order of 4−5 times narrower than typical spectra obtained for bulk samples,[22] and attests to the high degree of enrichment and purity achieved through the DGU separation.

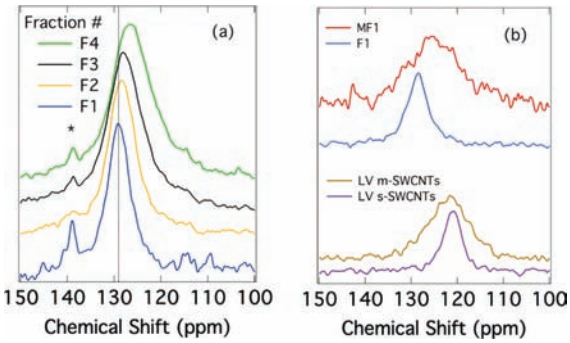

Figure 3. (a) ^{13}C NMR spectra of F1−F4. The dashed black line is a guide for the eye, demonstrating the progressive shift to lower frequency as the diameter distribution broadens to include larger diameter SWCNTs and metallic SWCNTs. (b) ^{1}H−^{13}C CP-MAS spectra of ^{13}C-labeled CoMoCAT SWCNT samples: MF1 (red) and F1 (blue); ^{13}C-labeled LV SWCNT samples: 94% m-SWCNTs (brown) and 92% s-SWCNTs (purple). The asterisk indicates the unsaturated impurities present in the polyethylene plugs.

To study the NMR spectra in more detail, each spectrum in Figure 3 was deconvoluted into either multiple or single Lorentzian peak(s) (Figure 4a−c). The ^{13}C resonance for F1, shown in Figure 4a, is fit well with one Lorentzian centered at 129 ppm (fwhm =5.4 ppm). In contrast, the ^{13}C resonance for the F4 sample, shown in Figure 4c, requires two Lorentzians: one centered at 127.3 ppm (fwhm =7.8 ppm) and one centered at 123.6 ppm (fwhm =10.5 ppm). The spectrum for MF1 is successfully fit with a single Lorentzian, centered at 125.1 ppm (fwhm =13.7 ppm). We interpret the spectral fits using the following model. The narrow 129.0 ppm peak for F1 is easily assigned to s-SWCNTs on the basis of the very narrow diameter and chirality distribution, dominated by the (6,5) s-SWCNT (Figure 2). Similarly, the metal-enriched MF1 sample, dominated by m-SWCNTs, displays a single broad peak shifted to lower frequency relative to the semiconducting (6,5) SWCNTs in F1. As shown in Figure 4c, the ^{13}C resonance for the F4 sample contains two populations of SWCNTs, represented by a narrow and broad component. The F1 and MF1 samples allow us to assign the narrow peak at 127.3 ppm to s-SWCNTs and the broader peak at 123.6 ppm to m-SWCNTs. The relative areas of the peaks (2:1) suggests a semi−metal ratio of ∼2:1, matching the expected statistical ratio of a random distribution. The larger fwhm for the s-SWCNT component of F4 (relative to F1) makes intuitive sense if we assume that the chemical shift varies as a function of diameter, as theoretically predicted,[16,17] meaning a distribution of diameters will have a distribution of chemical shifts. Indeed, Figure 4d demonstrates that the width of the isotropic ^{13}C peak assigned to s-SWCNTs scales directly with the width of the diameter distribution obtained by PLE analysis (Figure 2c).

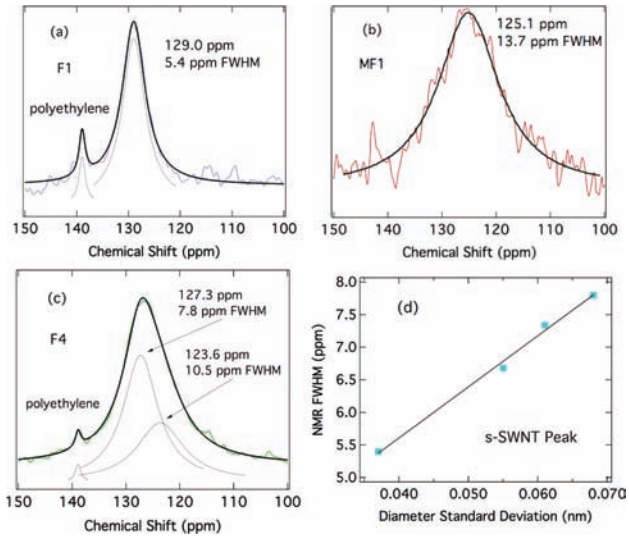

Figure 4. (a−c) Single- or multi-Lorentzian fits to samples F1, MF1, and F4, respectively. Fits for F2 and F3 are shown in the Supporting Information. (d) Plot of NMR fwhm (as obtained through the Lorentzian fitting routine) to the standard deviation of the diameter distribution (Δd, as obtained from PLE plots) for the peak assigned to s-SWCNTs.

Initial semiempirical calculations predicted a large diameter-independent chemical shift difference of ∼11 ppm between m-

dx.doi.org/10.1021/ja211181q | J. Am. Chem. Soc. 2012, 134, 4850−4856

and s-SWCNTs.[20] However, more recent first-principles computations have converged on a diameter dependence of the SWCNT ^{13}C chemical shift that follows the generalized functional form

$$\delta(\text{ppm}) = A(\lambda)/D^{\alpha} + B \quad (4)$$

where D is the tube diameter, B is the chemical shift limit for infinite diameter, and $A(\lambda)$ is a constant that depends on the nanotube family.[16] The values for A, B, and α in eq 4 vary significantly, depending on the particular calculation, and are summarized in Table S1 and Figure S5 of Supporting Information for the three most detailed theoretical reports available.[15−17]

To determine the appropriate scaling relationship for the SWCNT ^{13}C chemical shift, we plotted our experimental data against the theoretically predicted chemical shift values from references 15−17. A full comparison to references 15−17 is found in the Supporting Information.[36] Figure 5 compares our

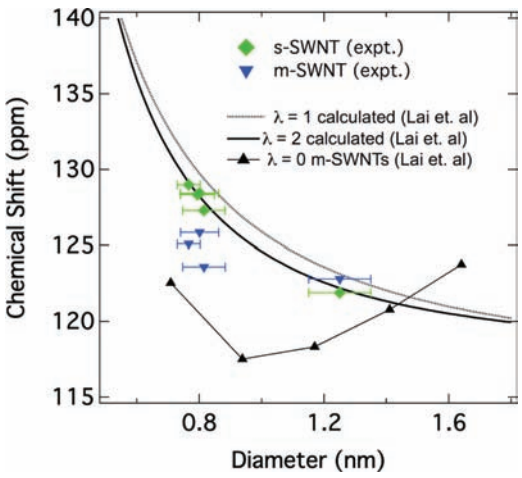

Figure 5. Plot of ^{13}C chemical shift as a function of SWCNT diameter for s- and m-SWCNTs. Experimental points, obtained in this study, are given as green diamonds (s-SWCNTs) and blue triangles (m-SWCNTs). Lines show calculated diameter dependence of chemical shift from Lai et al. for λ = 2 s-SWCNTs (black), λ = 1 s-SWCNTs (gray), and λ = 0 m-SWCNTs (black triangles). Detailed figure in Supporting Information denotes sample number for each sample.

experimental data with the theoretical predictions from Lai et al.,[17] for which we found the best agreement. Specifically, our data for s-SWCNTs follow the λ = 2 family dependent curve (solid black line) predicted by Lai et al.[17] Because of inherent uncertainties associated with the theoretical predictions and the limited number of data points, we hesitate in emphasizing the *quantitative* agreement of our data to these calculations. However, our data are the first to demonstrate that the generalized functional form of eq 4 predicts the *qualitative* dependence of the ^{13}C chemical shift on s-SWCNT diameter. Additional samples highly enriched in other single species, as well as further refinements in theoretical calculations, are needed to fully quantify this diameter dependence.

The data in Figure 5 also allow for the evaluation of how the SWCNT electronic structure (i.e., metallic versus semiconducting) affects the ^{13}C chemical shift and how this effect varies with diameter. The black triangles plot the computed chemical shifts for five $(n,0)$ λ = 0 metallic SWCNTs.[17] The calculations shown in Figure 5 predict that the chemical shift for s- and m-SWCNTs would be nearly overlapping at a diameter of ∼1.4 nm, but at small diameters such as ∼0.8 nm, the chemical shift for m-SWCNTs would be shifted to lower frequency relative to the small diameter s-SWCNTs. Our experimental data qualitatively confirm this trend. The ^{13}C chemical shifts for both s- and m-SWCNTs with $\langle d \rangle$ ∼1.25 nm are nearly equivalent, with the large diameter m-SWCNTs shifted slightly to higher frequency relative to the equivalent diameter s-SWCNTs. In contrast, when $\langle d \rangle$ is reduced to between 0.77 and 0.82 nm, the observed ^{13}C chemical shift for the m-SWCNTs is shifted to lower frequency by 3−4 ppm relative to the s-SWCNTs with similar $\langle d \rangle$.

We note that although our experimental data confirm the generally predicted trend of increasing chemical shift differences for m- versus s-SWCNTs with decreasing diameter, the magnitude observed experimentally is much less than that predicted by first-principles computations. For the diameter range explored here experimentally, both Zurek et al.[16] and Lai et al.[17] predict that the λ = 0 family should be shifted to lower frequency by ∼8 ppm relative to the λ = 2 family, while the experimentally observed difference is only ∼4 ppm. It is important to appreciate that the m-SWCNTs expected in the population distributions in our study are proximal to the (6,5) SWCNT and thus encompass chiral and armchair m-SWCNTs (Figure 2d), not the zigzag m-SWCNTs computed by first-principles computations. Additionally, we note that there is a high degree of uncertainty associated with the computed chemical shifts of m-SWCNTs due to the large unit cell that must be addressed for convergence. These considerations prohibit us from a rigorous quantitative comparison of our data to first principles calculations. However, we hope that the qualitative comparisons made here, using samples with well-characterized electronic structures, serve as a starting point for future refinement of the quantitative correlation between theory and experiment.

Finally, for both the small diameter CoMoCAT SWCNTs and the large diameter LV SWCNTs, the isotropic peak for the m-SWCNTs has a fwhm roughly double that of s-SWCNTs with similar $\langle d \rangle$. The reason for this broadening is unclear but is likely related to coupling of the ^{13}C nuclear spins to electron spins of free carriers, as was seen recently for heavily doped SWCNTs.[34] To our knowledge, such differences have not been predicted by first-principles calculations.

4. CONCLUSION

In conclusion, we have presented the first rigorous study of the effects of both diameter and electronic structure on the ^{13}C chemical shift in SWCNTs, using SWCNTs highly enriched by DGU and labeled with ^{13}C. We hope that the results displayed here will aid in the fundamental understanding of the physical principles governing the ^{13}C chemical shift in SWCNTs and can help to refine future computational efforts. Beyond the fundamental knowledge of the SWCNT ^{13}C chemical shift accessible through such samples, a number of applied studies could benefit from the DGU-separated ^{13}C-labeled SWCNTs demonstrated here. In particular, we suggest the incorporation of ^{13}C-labeled SWCNTs into a variety of different separation protocols, such that the resulting SWCNTs can be subjected to detailed multidimensional NMR analyses to understand the interfacial interactions between SWCNTs with known (n,m) indices and molecules such as, DNA,[12,13] diazonium salts, and anionic/cationic surfactants[9−11] typically utilized for separations. Furthermore, type-separated ^{13}C-labeled SWCNTs could provide detailed information regarding the molecular ordering

dx.doi.org/10.1021/ja211181q | J. Am. Chem. Soc. 2012, 134, 4850−4856

and noncovalent interactions occurring at important interfaces, such as those between SWCNTs and conducting polymers, fullerenes, or inorganic semiconductor surfaces.

■ ASSOCIATED CONTENT

Supporting Information

Determination of the MF1 population distribution, solution-phase Raman spectra of samples F1−F4, PLE maps of samples F1−F4, multi-Lorentzian fitting of F2 and F3, and a detailed comparison of experimental ^{13}C chemical shifts to available theoretical predictions. This material is available free of charge via the Internet at http://pubs.acs.org.

■ AUTHOR INFORMATION

Corresponding Author

chaiwat.engtrakul@nrel.gov; jeffrey.blackburn@nrel.gov

Notes

The authors declare no competing financial interest.

■ ACKNOWLEDGMENTS

Raw CoMoCAT SWCNTs were supplied by the University of Oklahoma. SWCNT separation, spectroscopy, and NMR characterization was performed at NREL and was supported by the Solar Photochemistry program of the U.S. Department of Energy, Office of Science, Basic Energy Sciences, Division of Chemical Sciences, Geosciences and Biosciences, under Contract No. DE-AC36-08GO28308 to NREL.

■ REFERENCES

(1) Diederich, F.; Whetten, R. L.; Thilgen, C.; Ettl, R.; Chao, I.; Alvarez, M. M. *Science* **1991**, *254*, 1768.
(2) Reed, C. A.; Kim, K.-C.; Bolskar, R. D.; Mueller, L. J. *Science* **2000**, *289*, 101.
(3) Troshin, P. A.; Avent, A. G.; Darwish, A. D.; Martsinovich, N.; Abdul-Sada, A. a. K.; Street, J. M.; Taylor, R. *Science* **2005**, *309*, 278.
(4) Kurotobi, K.; Murata, Y. *Science* **2011**, *333*, 613.
(5) Zhang, L.; Yang, J.; Edwards, C. L.; Alemany, L. B.; Khabashesku, V. N.; Barron, A. R. *Chem. Commun.* **2005**, 3265.
(6) Alemany, L. B.; Zhang, L.; Zeng, L.; Edwards, C. L.; Barron, A. R. *Chem. Mater.* **2007**, *19*, 735.
(7) Zeng, L.; Alemany, L.; Edwards, C.; Barron, A. *Nano Res.* **2008**, *1*, 72.
(8) Wang, H.-J.; Xi, X.-K.; Kleinhammes, A.; Wu, Y. *Science* **2008**, *322*, 80.
(9) Arnold, M. S.; Green, A. A.; Hulvat, J. F.; Stupp, S. I.; Hersam, M. C. *Nat. Nanotechnol.* **2006**, *1*, 60.
(10) Green, A.; Duch, M.; Hersam, M. *Nano Res.* **2009**, *2*, 69.
(11) Liu, H.; Nishide, D.; Tanaka, T.; Kataura, H. *Nat. Commun.* **2011**, *2*, 309.
(12) Tu, X.; Manohar, S.; Jagota, A.; Zheng, M. *Nature* **2009**, *460*, 250.
(13) Tu, X.; Hight Walker, A. R.; Khripin, C. Y.; Zheng, M. *J. Am. Chem. Soc.* **2011**, *133*, 12998.
(14) Saito, R.; Dresselhaus, G.; Dresselhaus, M. S. *Physical Properties of Carbon Nanotubes*; Imperial College Press: London, 1998.
(15) Marques, M. A. L.; d'Avezac, M.; Mauri, F. *Phys. Rev. B* **2006**, *73*, 125433.
(16) Zurek, E.; Autschbach, J. *Int. J. Quantum Chem.* **2009**, *109*, 3343.
(17) Lai, L.; Lu, J.; Song, W.; Ni, M.; Wang, L.; Luo, G.; Zhou, J.; Mei, W. N.; Gao, Z.; Yu, D. *J. Phys. Chem. C* **2008**, *112*, 16417.
(18) Zurek, E.; Autschbach, J. In *Computational Nanoscience*; Bichoutskaia, E., Ed.; Royal Society of Chemistry: Cambridge, 2011; p 279.
(19) Zurek, E.; Pickard, C. J.; Walczak, B.; Autschbach, J. *J. Phys. Chem. A* **2006**, *110*, 11995.
(20) Latil, S.; Henrard, L.; Goze Bac, C.; Bernier, P.; Rubio, A. *Phys. Rev. Lett.* **2001**, *86*, 3160.
(21) Engtrakul, C.; Davis, M. F.; Mistry, K.; Larsen, B. A.; Dillon, A. C.; Heben, M. J.; Blackburn, J. L. *J. Am. Chem. Soc.* **2010**, *132*, 9956.
(22) Abou-Hamad, E.; Babaa, M. R.; Bouhrara, M.; Kim, Y.; Saih, Y.; Dennler, S.; Mauri, F.; Basset, J. M.; Goze-Bac, C.; Wagberg, T. *Phys. Rev. B* **2011**, *84*, 165417.
(23) Ghosh, S.; Bachilo, S. M.; Simonette, R. A.; Beckingham, K. M.; Weisman, R. B. *Science* **2010**, *330*, 1656.
(24) Ju, S.-Y.; Kopcha, W. P.; Papadimitrakopoulos, F. *Science* **2009**, *323*, 1319.
(25) Ferguson, A. J.; Blackburn, J. L.; Holt, J. M.; Kopidakis, N.; Tenent, R. C.; Barnes, T. M.; Heben, M. J.; Rumbles, G. *J. Phys. Chem. Lett.* **2010**, *1*, 2406.
(26) Holt, J. M.; Ferguson, A. J.; Kopidakis, N.; Larsen, B. A.; Bult, J.; Rumbles, G.; Blackburn, J. L. *Nano Lett.* **2010**, *10*, 4627.
(27) Yang, C.; Hu, J. G.; Heeger, A. J. *J. Am. Chem. Soc.* **2006**, *128*, 12007.
(28) Nieuwendaal, R. C.; Snyder, C. R.; Kline, R. J.; Lin, E. K.; VanderHart, D. L.; DeLongchamp, D. M. *Chem. Mater.* **2010**, *22*, 2930.
(29) Alvarez, W. E.; Pompeo, F.; Herrera, J. E.; Balzano, L.; Resasco, D. E. *Chem. Mater.* **2002**, *14*, 1853.
(30) Resasco, D. E.; Alvarez, W. E.; Pompeo, F.; Balzano, L.; Herrera, J. E.; Kitiyanan, B.; Borgna, A. *J. Nanopart. Res.* **2002**, *4*, 131.
(31) Resasco, D. E.; Herrera, J. E.; Balzano, L. *J. Nanosci. Nanotechnol.* **2004**, *4*, 398.
(32) Dillon, A. C.; Gennett, T.; Jones, K. M.; Alleman, J. L.; Parilla, P. A.; Heben, M. J. *Adv. Mater.* **1999**, *11*, 1354.
(33) Engtrakul, C.; Davis, M. F.; Gennett, T.; Dillon, A. C.; Jones, K. M.; Heben, M. J. *J. Am. Chem. Soc.* **2005**, *127*, 17548.
(34) Mistry, K. S.; Larsen, B. A.; Bergeson, J. D.; Barnes, T. M.; Teeter, G.; Engtrakul, C.; Blackburn, J. L. *ACS Nano* **2011**, *5*, 3714.
(35) McDonald, T. J.; Jones, M.; Engtrakul, C.; Ellingson, R. J.; Rumbles, G.; Heben, M. J. *Rev. Sci. Instrum.* **2006**, *77*, 053104.
(36) See Supporting Information for additional details.
(37) Doorn, S. K.; Heller, D. A.; Barone, P. W.; Usrey, M. L.; Strano, M. S. *Appl. Phys. A: Mater. Sci. Process.* **2004**, *78*, 1147.
(38) Strano, M. S.; Doorn, S. K.; Haroz, E. H.; Kittrell, C.; Hauge, R. H.; Smalley, R. E. *Nano Lett.* **2003**, *3*, 1091.

■ NOTE ADDED AFTER ASAP PUBLICATION

Equation 4 contained errors in the version published ASAP on February 28, 2012; the correct version reposted February 29, 2012.